Interaction profiles and stability of rigid and polymer-tethered lipid bilayer models at highly charged and highly adhesive contacts

Pierluigi Bilotto,[†,¶] Maximilian Lengauer,[†,¶] Jakob Andersson,[‡] Ulrich Ramach,[†,§] Laura L.E. Mears,[†] and Markus Valtiner[*,†]

†*Vienna University of Technology, Institute of Applied Physics, Vienna, 1040, Austria*

‡*Austrian Institute of Technology, Vienna, Austria,*

¶*these authors contributed equally to this work*

§*CEST Kompetenzzentrum für elektrochemische Oberflächentechnologie, Wiener Neustadt, 2700, Austria*

E-mail: valtiner@iap.tuwien.ac.at

Abstract

Understanding interaction force versus distance profiles of supported lipid bilayers (SLBs) is relevant to a number of areas which rely on these model systems, including e.g. characterization of ligand/receptor interactions or bacterial adhesion. Here, the stability of 4 different SLB architectures was compared using the surface forces apparatus (SFA) and atomic force microscopy (AFM). Specifically, the outer envelope of

the bilayer systems remained constant as 1,2-dipalmitoyl-sn-glycero-3-phosphocholine (DPPC). The inner layer was varied between DPPC and 1,2-dipalmitoyl-3-trimethyl-ammonium-propane (DPTAP), both on mica and self-assembled monolayers (SAMs) of hexadecanethiol and the polymer tethered di-phytanylglycerol-tetraethyleneglycol-lipoid acid (DPhyTL) on smooth gold surfaces. In that same order these gave an increasing strength of interaction between the inner layer and the supporting substrate and hence improved stability under highly adhesive conditions. Detachment profiles from highly charged and highly adhesive contacts were characterized and approach characteristics were fitted to DLVO models. We find increasing stability under highly adhesive loads, approaching the hydrophobic limit of the adhesive energy between the inner and outer layers for the SAM based systems. For all four SLBs we further compare AFM surface topographies, which strongly depend on preparation conditions, and the DLVO fitting of the SFA approach curves find a strong charge regulation behaviour during interaction, dependent on the particular model system. In addition, we find undulation characteristics during approach and separation. The increased stability of the complex architectures on a gold support make these model systems an ideal starting point for studying more complex strongly adhesive/interacting systems, including for example ligand/receptor interactions, bio-sensing interactions or cell/surface interactions.

Introduction

Biophysical interactions on cell membranes can be well modelled experimentally using supported lipid bilayers (SLBs) as an excellent system for mimicking complex cell membranes. SLBs are particularly useful for characterizing membrane/membrane, membrane/substrate or ligand/receptor interactions in biomimetic systems. For example, SLBs can be used to build-up biosensing devices based on ligand/receptor interactions,[1] or they can mimic cell-cell interaction processes.[2] Specifically the surface forces apparatus (SFA) has been established

as a unique tool for lipid bilayer experiments to measure force versus distance characteristics during approach and separation of lipid bilayers, e.g. for quantifying ligand/receptor interactions or bilayer fusion and hemifusion.[3–7] Alternatively SLBs can be used as a supporting system for polymers enabling the formation of mushroom and brush regimes with controlled density and functionality,[8–10] allowing fundamental interactions between functional groups and surfaces to be probed with the SFA.

In all applications the stability of an SLB system is central, and force probe experiments provide a detailed insight into the stability of SLBs. In a DPPC bilayer versus DPPC bilayer contact the stability has been measured using SFA by Orozco-Alcarez and Kuhl,[6] finding a work of adhesion proportional to $0.5\,\mathrm{mJ/m^2}$. Benz *et al.*[11] used a combination of SFA and AFM on a bilayer versus bilayer system with DLPE/DPPE as the outer and inner layers respectively. For their most densely packed or "saturated" bilayers, repeated force-distance measurements consistently reached the same hard wall contact bilayer thickness, even at pressures over 100 MPa. A similar work of adhesion compared to the DPPC-DPPC contact, $W \approx 0.5\,\mathrm{mJ/m^2}$, was found. In contrast, when holes in one or both layers were present in the SLB and identified in AFM, with increased applied force the two bilayers' structure broke down and hemifusion of the layers occurred (and hence an adhesive, JKR contact) even if initially a non-adhesive (Hertzian) contact was found. The adhesion values increased dramatically into the high adhesion regime, between $15\,\mathrm{mJ/m^2}$ to $21\,\mathrm{mJ/m^2}$ for $18\,\%$ to $30\,\%$ defect area.

In this work we are interested in two aspects of SLB systems. First, we aim to develop a lipid bilayer model system for SFA that is defect free (e.g. no holes) and stable under electrochemical conditions, offering the future possibility to charge/discharge membranes during interaction force measurements, or *vice versa* to measure charge and discharge during interaction. In this direction SLB-systems already established for biosensing devices are an ideal starting point.[12] Second, we aim to improve SLB stability under highly adhesive conditions, which are to be expected not only in electrochemical systems but also in certain

cell processes. In this work, we define high adhesion to be values above $\sim 15\,\mathrm{mJ/m^2}$ as these are the values that occur for processes, such as hemifusion of bilayers, and hence are biologically significant for understanding events like membrane fusion.[2,5] The interaction between a single lipid bilayer on one side and a solid surface, without modifications on the other is less commonly investigated,[13,14] but provides a simple experimental systems where the contact is likely to be highly adhesive and where stability can be tested under extreme conditions. Two investigations of such an SLB against a hydrophilic surface, silica and mica respectively, have been made experimentally by Anderson *et al.*,[13] and using Grand Canonical Monte Carlo (GCMC) simulations by Pertsin and Grunze,,[14] with different conclusions. In the experimental measurements, in water only a repulsive force was observed during the approach of silica to the SLB on mica. However, the simulations predict that as the separating distance decreases there is an attractive force between mica and the SLB leading to a jump into contact. Within the simulations, undulations and spontaneous protrusions of molecules from the SLB were observed. It is unclear whether differences in surface topography, lipid head group or surface material should result in such changes in the force profiles from the two different approaches.

Here, we compare force profiles of different SLB models facing an atomically smooth mica surface (see **Figure 1**) with the theoretical work of Pertsin and Grunze[14] and the experimental data of Anderson with SLBs facing silica.[13] Further, we compare the stability of classic solid supported bilayer models systems with two alternative support methods based on self-assembly chemistry on gold for the inner leaflet of an SLB (see again **Figure 1**). Specifically, we compare the classic inner layer anchoring on silica based materials (e.g. mica, or glass) via (1) uncharged lipids with (2) anchoring via a positively charged lipid, and anchoring via two electrochemically polarizable systems including (3) a rigid and hydrophobic linear C16-alkanethiol self-assembled monolayer (SAM) as well as (4) a flexible SAM anchored and polymer-tethered lipid layer, di-phytanylglycerol-tetraethyleneglycol-lipoid acid, better known as DPhyTL.

We apply similar methods to Benz *et al.*[11] to test the stability of SLBs contacting a highly charged and adhesive solid surface, namely mica. Specifically, we compare AFM surface topographies, and force versus distance characteristics using the SFA. We find undulation forces, and charge regulation during interaction, which strongly depend on preparation conditions and the particular model system, respectively. We also find an increased long-term stability under highly adhesive conditions, and ideal electrochemical characteristics of a biomembrane for the DPhyTL system, making this model system for SFA an ideal starting point for studying more complex strongly adhesive/interacting systems. For instance, DPhyTL has been extensively used in other fields to assemble various model membrane architectures that have been applied to the study of bacterial toxins such as Gramicidin,[15] alpha-hemolysin,[16] valinomycin,[17] the interaction of silver nanoparticles with cellular membranes[18] and to mimic the outer membrane of gram-negative bacteria.[19]

Experimental Section

Materials

The lipids used in this work were 1,2-dipalmitoyl-sn-glycero-3-phosphocholine (DPPC) and 1,2-dipalmitoyl-3-trimethylammonium-propane (DPTAP), purchased from Avanti Polar Lipids. The lipids were dissolved in pure chloroform from Carl Roth (assay: $\geq$ 99.9 %), with lipid mass concentrations of 1 mg/mL for DPPC and 0.25 mg/mL for DPTAP.

The other chemicals were sourced as follows: sodium chloride from Carl Roth (assay: $\geq$ 99 %), n-hexane from Carl Roth (assay: $\geq$ 98%), ethanol $\geq$ 99.9% pure from VWR, hexadecanthiol ($C_{16} -$ SH, assay: 99%) from Sigma Aldrich, Inc., di-phytanylglycerol-tetraethyleneglycol-lipoid acid (DPhyTL) from Celestial Synthetics, EPO-TEK heat curable glue (EPO-TEK 377) from Epoxy Technology and UV curable glue (NOA 81) from Norland Products Inc. Milli-Q water (Milli - pore, TOC value < 2 ppb, resistivity > 18 MΩ) was used throughout.
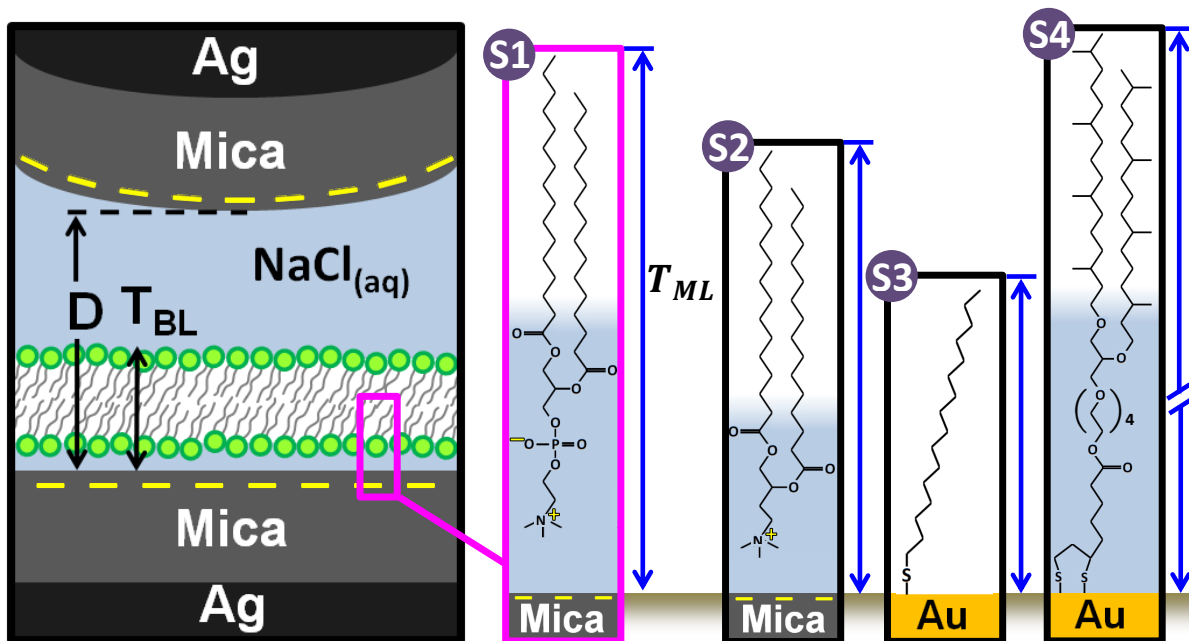
Figure 1: **SFA configuration and chemical structures of the inner layers.** The SFA configuration is shown for system S1. The bilayer system was placed on one side and a blank mica surface was used as the apposing surface. All samples were immersed in 8 mM NaCl. The silver layers form the interferometric cavity. The distance D and the bilayer thickness T_{BL}, is defined in the schematic. Chemical structures of the inner layers - System S1: DPPC/DPPC on mica; System S2: DPPC/DPTAP on mica; System S3: DPPC/ hexadecanethiol on Au; System S4: DPPC/DPhyTL on Au.[20] T_{ML} indicates the monolayer thickness.

Supported Lipid Bilayers (SLBs)

Langmuir-Blodgett deposition of SLBs A Langmuir-Blodgett (LB) trough, built by Dr. Hans Riegler (Max-Planck Institute for Colloid and Interface Research, Potsdam), with a deep central well for sample transfer was used for the LB measurements and depositions. The LabView written control software for processing the signals from the barrier motor and from the Wilhelmy plate was kindly provided by Dr. Michael Kappl from the Max Planck Institute for Polymer Research. Our studies with the LB trough were carried out with lipid amounts of 0.46 µMol to 1.09 µMol. For DPPC/DPTAP mixtures, the defined volumes of lipid containing solutions were dropped onto the water surface successively. Mixture molar

ratios (DPPC:DPTAP) applied were 37 : 63, 47 : 53 and 81 : 19. At least 4 independent surface pressure-area isotherms were measured for each mixture to obtain the respective lipid area per molecule at a surface pressure of $\Pi = 42\,\mathrm{mN/m}$ (**Figure S1**). Those gave, together with the defined mixture ratios, a direct relation to the charge densities of the lipid monolayers.

For depositing lipid layers onto substrates, the Langmuir-Blodgett method was applied, i.e. the substrate was moved vertically with $15\,\mu\mathrm{m/s}$ through the lipid monolayer (out of/into bulk water for inner/outer layer deposition), at a pre-adjusted surface pressure of $\Pi = 42\,\mathrm{mN/m}$. Hence, the outer lipid layer deposition ended with the sample fully submerged under water, ready for underwater transfer to the relevant measurement cell.

SAM based systems We prepared the two different SAM based systems as follows. The hexadecanthiol ($C_{16} - \mathrm{SH}$) was deposited by immersion in a 1 mM solution in pure filtered ethanol (0.2 μm pore size) onto a smooth gold film substrate (template striped from atomically smooth mica) glued to a cylindrical or flat disk depending on whether it was for an SFA or AFM experiment. We kept the substrate in solution for 1 hour in the dark and at constant room temperature. After deposition, the substrate was sonicated consecutively in pure n-hexane and pure filtered ethanol. For the DPhyTL deposition a 0.1 mg/mL DPhyTL solution was prepared in pure ethanol and into which the gold substrate was immersed following the same protocol as described for the C_{16} deposition. The outer layer of our sample was always DPPC, deposited as a monolayer with the Langmuir Blodgett technique described above, with the sample ending inside the trough.

Atomic force microscopy

The atomic force microscopy was performed with an Asylum Research Cypher ES Atomic Force Microscope (Oxford Instruments) in amplitude modulation mode (AM-AFM). All samples were imaged in 8 mM NaCl solution. In liquid environments, cantilevers with a

given resonance frequency of 2000 kHz (Nanosensors, product name: Arrow UHFAuD) were used. For measuring in air, silicon cantilevers with resonance frequency of about 330 kHz (Nanosensors, product name: PPP-NCHAuD) were applied. For both cantilever types the back side was gold coated for photothermal excitation (blueDrive mode). For data processing and analysis of the topography data, the Asylum software package was used. For image levelling, second order polynomial fitting was applied. The variation of hole depth of the DPPC bilayer on mica support was based on the analysis of 74 defect structures in 5 different areas of the same sample.

Surface Forces Apparatus

Two different Surface Forces Apparatus (SFA) were used for normal force measurements in transmission mode. The first one is the SFA 2000 (SurForce LLC, Santa Barbara,CA) utilized to perform the experiments on lipid bilayers deposited mica. The second one is a new SFA prototype developed in our laboratories. It introduces advantages in terms of the optics, alignment and sample handling during the experiment.[21] Mica sheets used in these experiments were hand-cleaved to provide sheets with an area of 5–10 cm^2 and uniform thickness raging from 3–5 μm. The edges of these sheets were melt-cut with a hot platinum wire. Using a PVD with a base pressure of $5 \times 10^{-7} mbar$ by BestTec (Berlin, Germany) the mica sheets were back silvered by electron beam deposition.

To perform the experiments with SLBs, the sheets were glued on cylindrical fused silica disks with a nominal radius curvature $R = 1–2$ cm using an UV curable glue. In the case of SAM based experiments, the substrates consisted of atomically smooth gold films (described in SAM based systems above). As in previous work, initially, substrates were glued with NOA81 (Norland adhesives, UV curable adhesive) however significant plastic deformation of the surface occurred during SFA experiments under highly adhesive load (contact deformation is shown in the SI, **Figure S2**). EPO-TEK 377 (Epotek Technologies Inc.), a heat cured glue, was identified and used (if not otherwise specified) as a harder alternative and

showed improvements to the smoothness of the gold in AFM (see SI, **Figure S3A** and**B**) and did not deform under highly adhesive loads. All measurements were performed in $8\,\text{mM}$ NaCl. Further details on the SFA technique are given in previous works.[21,22]

The SFA data analysis was performed with SFA Explorer a program developed in our laboratories that uses the multiple matrix method to simulate the multiple beam interferometry taking place in the SFA optical cavity, translating the measured spectra from the fringes of equal chromatic order (FECO) into absolute distances between the surfaces with uncertainty equal to $0.05\,\text{nm}$, and lateral resolution of $1.56\,\text{µm}$ per pixel.[21]

Results and Discussion

In this work we characterize the four different supported lipid bilayer (SLB) model systems, which have distinctly different inner-layer anchoring chemistry (S1 - S4), as shown in **Figure 1**. We test the force response for all model systems against a highly charged surface, as well as their stability upon de-adhesion from highly adhesive contacts. Topography and undulations of the bilayers were characterized with AFM imaging, and force distance profiles during approach and separation (de-adhesion) were recorded using the SFA.

Figure 2 shows the force versus distance characteristics recorded during approach of mica to the DPPC/DPPC system supported on a mica surface (labelled S1) for two consecutive profiles. In the first approach, when the surfaces touch for the first time, a long range electric double layer repulsion is followed by a jump to a distance $T_{BL} = 4.3 \pm 0.5\,\text{nm}$ corresponding to the DPPC bilayer thickness.[23] With increasing external force the bilayer is compressed, and the mica to mica distance reaches a minimum value of $D = 1.1 \pm 0.2\,\text{nm}$ at $F/R = 30\,\text{mN/m}$. This indicates that the bilayer does not maintain a stable thickness upon compression, which suggests an unstable bilayer under very moderate compression.

A further indication of instability of the S1 system is that in the second approach, a jump-in to $T_{BL}^{*} = 9.7 \pm 0.5\,\text{nm}$ occurred, which is about double the distance compared to
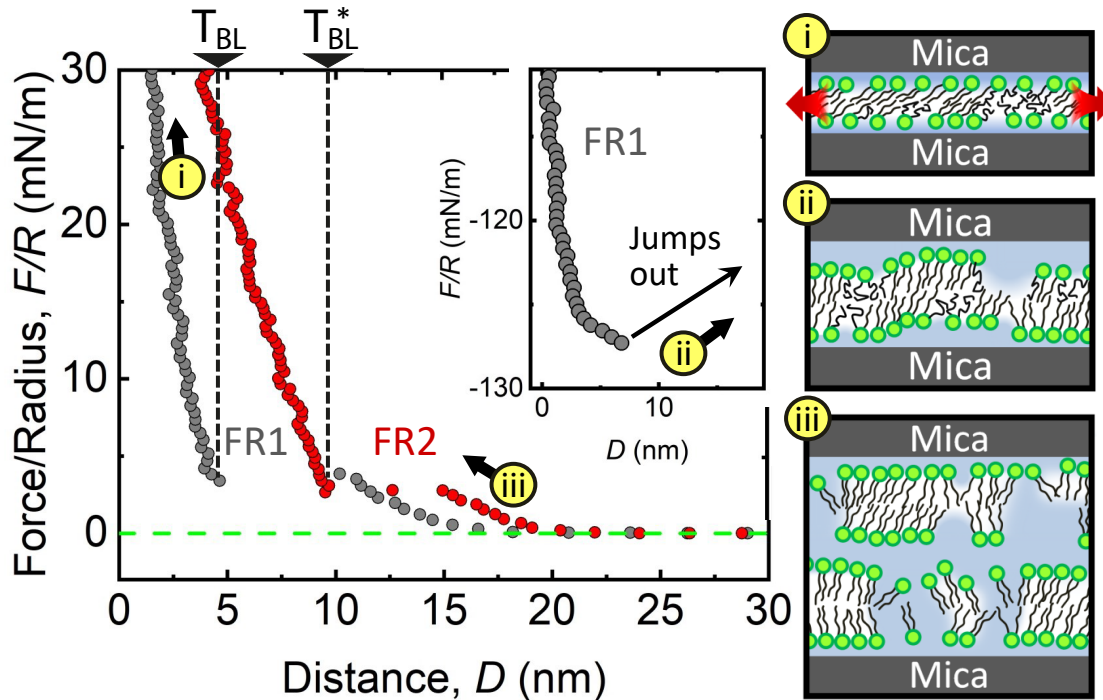
Figure 2: **DPPC/DPPC bilayer (S1) LB-deposited on muscovite mica.** Force-distance profile of the approaches from two sequential force runs of S1. The first is denoted FR1 (grey) and the second is FR2 (red). After the first profile jumps to a distance $D = T_{BL}$, representing the bilayer thickness in confinement, (i) the surfaces are in contact and a compressing force F_C is applied to the system, squeezing the bilayer. When the surfaces are moved apart, the bilayer adheres to both mica sheets, and an equal adhesion force, F_{Adh} acts at both interfaces. When the surfaces jump out of contact, (ii) the bilayer bridges the gap during separation before breaking and (iii) parts of the bilayer remain on both sides. As a consequence, the force profile is shifted to higher distances for FR2, and a jump-in to a distance $D = T_{BL}^*$ is observed, which has approximately double the value of T_{BL}.

the first force measurement. Also during the second approach increasing load resulted in a considerable compression of the confined material. This is not surprising and indicates that the bilayer was considerably damaged during the first separation. The molecular mechanism is depicted in the sketch of Figure 2 as follows: (i) When the system has been compressed

for the first time the bilayer is sandwiched between the two identical mica surfaces, with equal surface attraction to both sides of the bilayer. (ii) Due to the symmetry of the system (similar interaction of lipid head groups with both confining surfaces), during the jump-out it is likely that parts of the bilayer have remained in contact with the apposing mica surface, as indicated by the U-shaped force-versus distance characteristic during separation with a jump out of contact at about $D = 8\,\mathrm{nm}$, almost twice T_{BL} (inset in Figure 2). (iii) When the surfaces are then brought out of contact again, some lipids will remain attached to each of the two surfaces, i.e. some transfers from the original surface to the apposing one due to similar interaction strength with either side. For this reason, when the surfaces are brought together for a second time, the configuration will be similar to two bilayer island covered substrates interacting with each other, consequently jumping into an initial contact at a distance that is double the expected bilayer thickness.

It is possible to overcome this issue by choosing anchoring-lipids with a stronger interaction to the mica surface. A frequent choice for SFA experiments have been other zwitterionic lipids with a phosphatidylethanolamine (PE) termination to improve stability, relying on the strong interaction of the terminal primary amine of the PE group with mica.[11,24]

In the following we will show results of similar measurements with three different anchoring mechanism, including a positively charged lipid (DPTAP), which will work in a similar way compared to PE, with its charge providing additional interaction with the negative mica surface. Additionally we also tested two self assembled monolayers (SAMs) that have been used to modify surfaces for SLBs used in bio-sensing and other fields.[12,25] Although these SAM based systems do not follow the classical definition of an SLB, as only the outer leaflet is composed of lipid molecules, SLB will be used throughout for simplicity.

AFM topography of bilayer models. We first inspected all of the different architectures (labelled S1-S4, according to the anchoring) using AFM topography imaging as displayed in **Figure 3**. The sketches above represent our interpretations of the scan images.
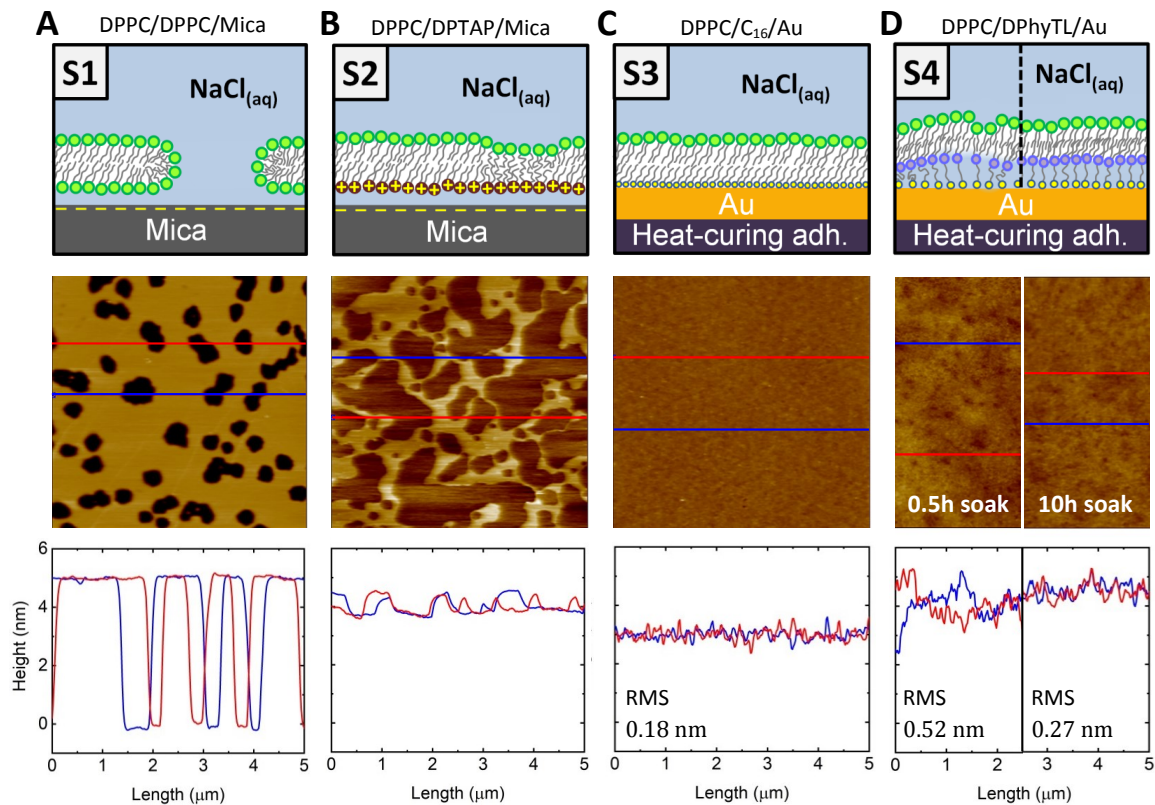
Figure 3: **AFM scan images of the lipid bilayer systems investigated.** Two height profiles are given below the images to represent the whole system. **(A)** System S1: Mica supported DPPC bilayer. Here, the height difference of the round-shaped defects is $5.15 \pm 0.03\,\mathrm{nm}$. **(B)** System S2: Mica supported DPPC/DPTAP bilayer. The height difference of the distinct regions is $0.40 \pm 0.03\,\mathrm{nm}$. **(C)** System S3: DPPC/hexadecanethiol bilayer on a gold substrate, prepared with EPO-TEK 377. **(D)** System S4: DPPC/DPhyTL bilayer on a gold substrate, prepared with EPO-TEK 377. The given RMS values for **C** and **D** were calculated from the line profiles shown. The sketches above show our interpretation of the obtained surface topographies.

The topography of S1 (**Figure 3A**) contained multiple round-shaped defects with a typical diameter of $600\,\mathrm{nm}$, uniformly distributed across the entire surface with depths between $3.65\,\mathrm{nm}$ and $5.25\,\mathrm{nm}$. Such defect structures are well known for similar SLB systems, and were shown to represent the thermodynamically equilibrated structure of the membrane at a constant temperature,[11] and similar defects were observed for similar SLBs by Hui *et al.*

using AFM.[26]

In contrast, as shown in **Figure 3B** the surface topography of the mica supported DPPC/DPTAP system (S2, see again **Figure** 1) showed no bilayer defects, but a division in bilayer regions with clear boundaries and a distinct height difference of typically 0.4 nm. This was observed in all AFM measurements on S2 and over several hours of measuring, which indicates a phase coexistence, in the range expected for this lipid.[27] Using a charged lipid (here DPTAP) as anchoring-lipid maximizes the electrostatic lipid-substrate attraction. In this case the surface charge densities of the inner lipid layer and the substrate have to match as closely as possible. For a gel-phase DPTAP film, i.e. the highest possible compression and hence charge per area, pressure isotherms (**see SI, Figure S1A and B)** at the water-air interface indicate that the mica surface charge can be compensated by about 95%, considering an ideal mica. The absence of holes or other large-scale defects in S2 aligns with the additional electrostatic attraction to the mica substrate.

In order to increase the binding energy between the SLB and the substrate, we further introduced two hydrophobic self-assembled monolayer (SAM) systems, that are covalently bound to the gold support, which also offers the future possibility to polarize the membrane in an electrochemical SFA.[28,29]

First, hexadecanethiol was applied as hydrophobic anchoring layer (i.e. inner layer of S3), as shown in Figure 1. This provides a uniform inner layer with high molecular packing density. An AFM scan image of S3 is shown in **Figure 3C**. The root mean square roughness of about RMS = 0.2 nm demonstrates the absence of defects in the system and a very flat surface topography. These undulations left in the system are shown to be situated in the bilayer itself, rather than within the inner, SAM layer underneath or the gold substrate layer which are defect free (see SI, **Figure S3B for gold** for direct comparison). No phase coexistence was observed on these layers, possibly due to the limited fluidity of the outer layer on this support, or due to other effects such as slightly different tilt angles imposed by the SAM which may in turn shift phase equilibria.

The second SAM system applied was DPhyTL as anchoring layer (S4), which has a gold-binding disulfide group linked to a highly-branched phytanyl lipid by a hydrophilic tetraethylenglycol (PEG4) polymer chain (see again Figure 1). The AFM scan image of the DPPC/DPhyTL system (S4) shown in **Figure 3D(left)** indicates a moderate coverage of large-scale undulations of the bilayer, resulting in a comparably higher RMS-value of about RMS = 0.5 nm. The origin of these undulations is located in the flexible anchoring layer, which is clear from our AFM measurements on the DPhyTL monolayer in aqueous solution (see SI: **Figure S3C**), showing the same undulating structures of the SAM. In addition, the gold substrate (see SI, **Figure S3B**) exhibits a negligible roughness of RMS = 0.05 nm. This system further shows randomly arranged defect structures of less than 1 nm depth. These defects were not observed in the DPhyTL monolayer (see SI, **Figure S3C**), and are hence consistent with a phase coexistence in the outer DPPC layer. Interestingly, and as shown in the comparison in **Figure 3D**, the large-scale undulations level-out considerably with extended immersion times in electrolytes for both an exposed DPhyTL monolayer and a fully formed SLB on DPhyTL, while the randomly arranged defect structures appear to be smaller in size but still visible. This indicates that the PEG4-chain, which is buried under the highly-branched lipid, needs an extended hydration time in aqueous electrolytes.

Interaction force profiles of SAM based bilayers. Comparing the two SAM based systems, S3 clearly gives a higher-quality surface topography. While, S4 has more undulations, bringing it closer to natural membranes, the PEG rehydration requires extended exposure to electrolytes (about 10 hours is sufficient for full PEG hydration). All systems S2, S3 and S4 show promising topography for providing a stable bilayer during force probe experiments and specifically under high adhesion. Here, we will now asses this by direct force probe experiments using the SFA. **Figure 4** shows the force versus distance characteristics of S3 and S4 approaching a mica surface recorded with the SFA. Briefly, measurements for S2 (not shown) facing a mica surface also demonstrated instability under high adhesion, with no

consistent thickness and adhesion reached over multiple measurements at the same contact. Results were qualitatively comparable but less severe compared to S1 shown in **Figure 2**.

Figure 4A displays the force versus distance characteristic for S3 facing a mica surface (see the top right inset of **Figure 4A**). First, the force profiles indicate a long range electric double layer repulsion scaling with the Debye length, a jump into contact from about $D = 6.5$ to $D = 3.7$ nm, and a further compression over about 0.5 nm before a final hard wall is reached. Second, the S3 system exhibits a perfect stability in terms of the hard wall thickness and reproducibility. In particular, we recorded a thickness (hard wall) at maximum compression of $T_{BL} = 3.16 \pm 0.06$ nm during the first force run (FR1), $T_{BL} = 3.17 \pm 0.06$ nm and $T_{BL} = 3.14 \pm 0.07$ nm during the second and the third force runs (FR2 and FR3). The thickness of similar bilayer systems has been investigated in previous work using neutron reflectivity[30] and molecular dynamics simulations.[31] In those works, the thicknesses ($T_{BL} = 4 \pm 1$ nm) are on average higher, with about 1 nm of the total thickness assigned to the hydrated head group. This difference is likely caused by the confinement, and consequent dehydration of the head group after the jump into a strongly adhesive contact of the S3 system. Further, one can see that all force runs of a single experiment exhibit identical interaction force profiles during approach of the S3 system and a mica surface, indicating excellent reproducibility.

Figure 4B shows three consecutive force versus distance characteristics of the S4 system facing a mica surface. The profiles of the different approaches show the same shape and they exhibit a defined jump in from about $D = 10$ nm into $D = 4.3$ nm, which corresponds to the thickness of the bilayer model. In contrast to S3 the force profiles indicate a lower electric double layer repulsion followed by a jump into a slightly attractive regime, and again a compression over about 0.5 nm into the repulsive hard wall.

At the maximum applied load the hard wall thickness of $T_{BL} = 4.3 \pm 0.5$ nm for S4 was stable over more than 5 repeated runs. As for the S3 system, the hard wall in contact is about 1 nm lower compared to values for uncompressed and hydrated DPhyPC/DPhyTLs

bilayer heights from neutron reflectivity studies,[32] and in the expected range for a confined bilayer under applied load.[6,8,11,23] This is consistent with confinement effects in SFA such as interdigitation, headgroup dehydration and polymer compression of the PEG4-tether in the present case. Moreover, this interpretation conforms with the AM-AFM measurements on S4: In **Figure 3D** the topography of the S4 bilayer shows undulations of the bilayer, which derive from the soft properties of the polymer (polyethyleneglycol, PEG) linker chains in the DPhyTL.
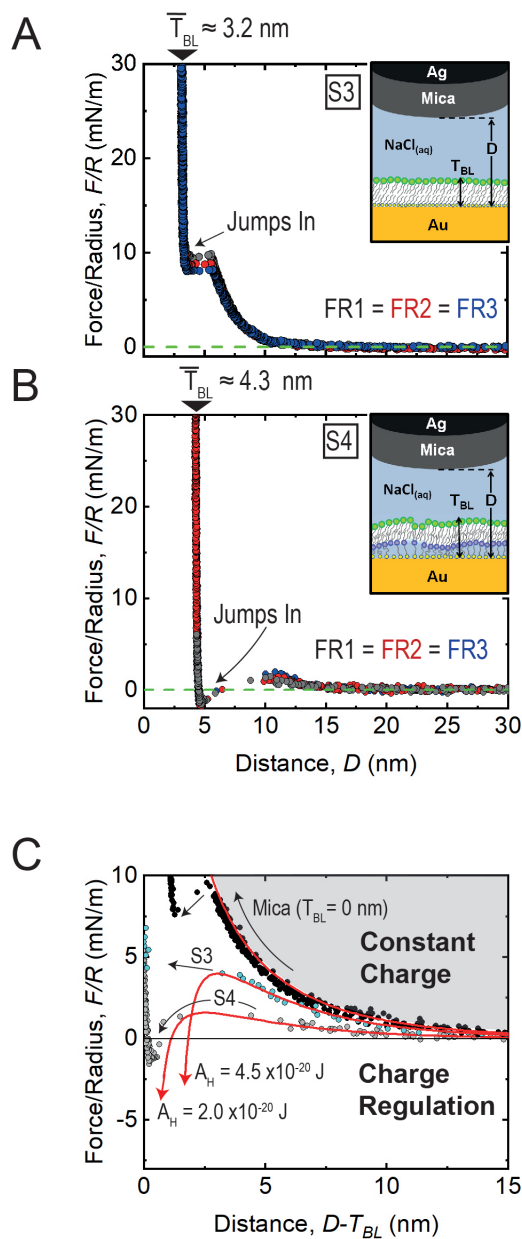
Figure 4: **Force-distance curve profiles obtained from SAM based SLBs. A** Force runs (FR) of system S3 (DPPC/C_{16}) deposited on gold facing a mica surface (schematic inset, top right). The force F/R is normalized by the curvature of the crossed-cylindrical surfaces. The averaged bilayer thickness measured is indicated by $\overline{T}_{BL}$. **B** Force runs (FR) of system S4 (DPPC/DPhyTL) on gold (schematic inset, top right). **C** Fit on the interaction forces of two mica surfaces brought into contact (black markers), S4 system against mica (grey markers) and S3 system against mica (blue markers). The abscissa is the distance between the two outer face of the surfaces taken in analysis. When no SLB is present, $T_{BL} = 0$ nm. The mica-mica curve is well fit by a constant charge solution of the DLVO function, while the SAM SLB systems are fit with a charge regulation solution, obtaining two different Hamacker constants A_H (see the text for more details).

17

As shown in **Figure 4C** the measured equilibrium force versus distance characteristics during approach of systems S3 and S4 against the highly charged mica can be fitted well at distances $D - T_{BL} > 2 - 3$ nm as a linear superposition of electric double layer, (F_{EDL}), and van der Waals, (F_{VDW}), interactions using the DLVO theory. Here, these systems are highly asymmetric in terms of their electric double layer properties, hence the electric double layer contribution is described using a Charge Regulation (CR) model for two asymmetric surfaces[33,34] as follows:

$$
\frac{F_{DLVO}}{R} = \frac{F_{VDW}}{R} + \frac{F_{EDL}}{R} = -\frac{A}{6(D - D_{VdW})^2}
$$
$$
+ 2\pi\epsilon\epsilon_0\kappa \frac{\left[2\,\psi_1\psi_2\,e^{-\kappa(D-D_{EDL})} + ((2\,p_1 - 1)\,\psi_2^2 + (2\,p_2 - 1)\,\psi_1^2)\,e^{-2\kappa(D-D_{EDL})}\right]}{1 - (2p_1 - 1)(2p_2 - 1)\,e^{-2\kappa(D-D_{EDL})}} \quad (1)
$$

where ψ_n indicates the potential at the diffusive layer for each of the surfaces in a 1:1 electrolyte solution, ϵ and ϵ_0 are the electric permittivity of water and the permittivity of free space, A_H is the Hamaker constant and κ is the inverse of the Debye length.[33,34] D_{EDL} and D_{VDW} describe the plane of origin of the individual force contributions. Specifically, for VDW contributions a shift of the plane of origin allows a simple modeling of layered systems, and EDL interactions originate from the diffuse layer interaction, which can hence be shifted by the thickness of the inner electric double layer.[35] The parameters p are charge regulation parameters and converge the interaction to the constant charge solution (CC) if $p = 1$ or to the constant potential solution (CP) if $p = 0$ for the respective surface. The principal plane of origin for the fitting is defined as the closest approach of the bilayer and mica, as $D_0 = D - T_{BL} = 0$. VDW or EDL shifts refer to this plane.

In our fitting approach we initially fit parameters for the mica surface in a symmetric experiment to fix the parameter p for mica. Hence, **Figure 4C** also shows the force distance characteristic measured across two approaching mica surfaces. The profile is highly repulsive during approach, shows a jump into a hard wall at about 1 nm. This is fully consistent with

a constant charge behaviour with the counter ions remaining within the contact zone. The 1 nm hard wall agrees well with a hydrated sodium layer confined between the hydrated mica surfaces. As can be seen in **Figure 4C**, the data can be well fitted with Equation 1 using a charge regulation parameter of $p_1 = p_2 = p_{mica} = 0.9$ and a diffuse double layer potential located at $D_{EDL} = 0.5\,\text{nm}$ of $\psi_1 = \psi_2 = \psi_{mica} = -71 \pm 4\,\text{mV}$, depending on the particular mica used. Hence, mica can be well described in terms of a constant charge surface down to distances of about $D = \frac{1}{\kappa}$, as expected. At smaller distances hydration effects overpower the DLVO contribution across symmetric mica versus mica force versus distance characteristics, which are not fitted here.

With this set of mica parameters, we can consistently fit the force versus distance characteristics for both the S3 and S4 systems while approaching a mica surface. Both bilayer models are well described by considerably lower charge regulation parameters. Specifically, the S3 and the S4 system are fitted well with $p = 0.4$ and $p = 0.35$ respectively. As such, these surfaces are characterized more closely by constant potential solutions. The diffuse layer potential of the S4 system is low at $\psi_{S4} = -27 \pm 2\,\text{mV}$. Utilizing Grahame's equation this corresponds to a charge density of $-0.03\,\text{Cm}^{-2}$, or one charge per $700\,\text{nm}^2$. This is about one charge per 10 lipid head groups on the surface, suggesting a charging of the neutral lipid by anion, here chloride, adsorption.

Interestingly, the diffuse layer potential of the S3 system is considerably higher at $\psi_{S3} = -53 \pm 2\,\text{mV}$, corresponding to a charge density of $-0.058\,\text{Cm}^{-2}$, or one charge per $275\,\text{nm}^2$. This indicates a considerably higher negative charging of the DPPC anchored to the SAM surface. This is consistent with an increased VDW attraction of the highly polarizable chloride ions to the surface, due to the substrate gold layer which is located about 3 nm below the surface for the S3 case, and more than 4.2 nm below the surface for the S4 case. This interpretation is also consistent with higher overall VDW interactions, and a larger jump into contact distance observed for the S3 system (see again the fit in **Figure 4C**). As already mentioned, at shorter separation distances below $D = $ 2-3 nm the surfaces deviate

from DLVO behaviour, which is that they show an instability and jump in to close contact, followed by a short range repulsion over 0.5 nm. The instability at $D = $ 7-10 nm seems to correlate with an overpowering of the electric double layer repulsion by attractive van der Waals interactions for the S3 and S4 system, with a larger effective Hamaker constant of the S3 system. This agrees well with the thinner film thickness and hence larger contribution of the underlying gold substrate. For the S4 system the short range repulsion can be fit reasonably well with either of the following two models: First, a short range exponential hydration repulsion with a quite short scaling length of 2-3 Å fits the data. Second, a $1/D^3$ dependence of a Helfrich like model[36] with a bending modulus $k_b = 2.5 - 5.0 \times 10^{-19}$ J fits the data slightly better and is in line with previous results.[37] The former may relate to the head group dehydration, while the latter is related to an undulation repulsion. On the basis of the current data we conclude that the short range repulsion maybe a superposition of both contributions, while it seems more likely that the repulsion after the jump is dominated by the damping of the natural undulations of the systems.[38]
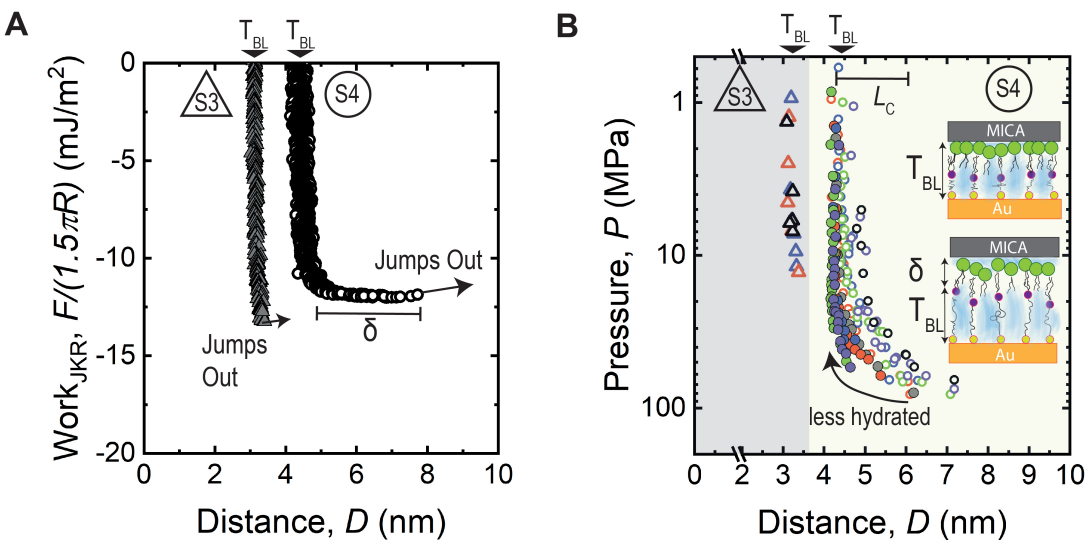

Figure 5: **Adhesion and pressure for SAM based systems. A** Force profiles during surface separation for S3 (triangles) and S4 hydrated (open circles). Before each jump out, the S4 system increases its thickness in confinement by a quantity δ while keeping the force constant. **B** Pressure measured as a function of the distance for S3 (triangles) and both S4 hydrated (open circles) and not hydrated (full circles) systems. The contour length L_C of the PEG system is displayed for comparison with δ (see inset sketch).

20

Figure 5 shows characteristic A) force (normalized by 1.5ΠR) and B) pressure versus distance profiles during separation for the two SAM based bilayers, S3 and S4, from mica respectively. In **Figure 5A** the points where the adhesive junctions break and the surfaces suddenly jump apart to some large distance are marked as "jumps out". Interestingly, both systems show a considerably different contact geometry and force versus distance characteristic during separation, and the S4 system shows a pronounced dependence on the preparation history, as follows.

First, in **Figure 5A** the normalized force versus distance characteristics for the S3 system show a distinct jump out from the bilayer thickness with a small $5\,\text{Å}$ extension from the hard wall at higher pulling forces. The measured adhesive force of $62 \pm 12\,\text{mN/m}$ is stable over three consecutive force runs at the same position. This suggests that the S3 supported bilayer remains stable upon multiple separations under high adhesive load. The $5\,\text{Å}$ extension may be due to increased undulations under high pulling forces, where they are not damped any longer, due to a change of the tilt angle during pulling, or due to rehydration of the headgroups just before adhesive separation. This we may only further clarify with an SFA/spectroscopy combinations. Quite in contrast, for the S4 system the force versus distance profiles display a pronounced gradual increase in the distance at constant force. This results in a plateau of constant force stretching a distance of approximately $\delta = 2.5\,\text{nm}$ for the hydrated S4 and $1.3 \pm 0.2\,\text{nm}$ for the not hydrated S4 just before the surfaces jump apart. The stretching distance δ can be 5–$8\,\text{Å}$ smaller, similar or 5–$10\,\text{Å}$ larger compared to the full contour length $L_C = 1.5\,\text{nm}$ of the PEG-chain in the system. The L_C is larger than the maximum polymer extension, by its compressed thickness, and is a relevant length-scale if polymer extension is the only active process during separation. Therefore, it is often taken as a reference for similar shapes observed for other tethered systems. Here the extension is more complex and depends on the preparation conditions, which will be discussed below (fourth).

S3 is hence acting as a rigid system without significant extension before contact sepa-

ration, a property that comes from the rigid C_{16} structure, which is strongly bound to the substrate propagating its rigidity to the entire bilayer through the densely formed SAM. As such, the S3 system can be treated as a JKR contact, and the work of adhesion can be directly evaluated from **Figure 5A**. In contrast, the S4 system indicates an extension of the system's thickness while still in adhesive contact, with a pronounced L-shape of the force versus distance profiles. This is comparable to more gradual U-shaped profiles observed for soft adhesive systems containing PEG chains for ligand/receptor probing.[8] This is consistent with a stretching of the system (PEG4) before adhesive failure occurs. As a result, the work of adhesion cannot be evaluated using the JKR model, and the measured forces cannot be immediately compared to the S3 model system. The S4 data are put on the same axes in **Figure 5A** for ease of comparison only.

Second, and as shown in **Figure 6**, this behaviour is also reflected in the contact geometry recorded in-situ with the SFA during separation. FECO recorded at the point of separation indicate an extended flat contact for the S3 system, and the area versus applied load curve shows a typical JKR shape (analysis not shown). The adhesion is also independent of the load applied during approach (See SI, **Figure S4**). However the S4 system indicates a strongly decreasing contact area during separation and hence increasing pressure, which is not consistent with the separation of a JKR contact, yet appears consistent with a peel-off at constant force. This is due to additional modes of deformation originating from soft and polymer-tethered the bilayer architecture.

Third, **Figure 5B** shows the data for S4 and S3 in terms of pressure (force/area) versus distance characteristics and compares both systems in terms of the adhesive pressure during separation. The direct comparison of the adhesive pressures and forces during separation suggests that both systems, S3 and S4, reach comparable adhesive forces of F/R = 60-80 mN/m or W_{JKR} = 12-14 mJ/m^2 (see again **Figure 5A and B**), while adhesive pressures are - as expected - much higher in the S4 case that separates by a peel-off mechanism, where the contact area decreases at constant force. It is interesting to note, that the distance for S4
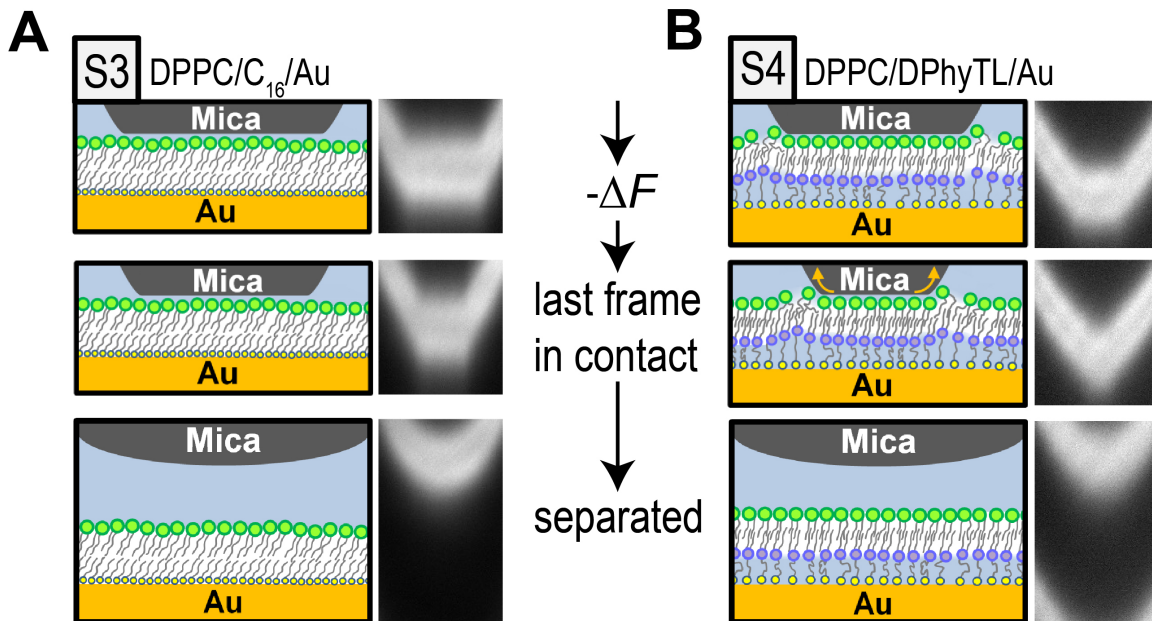
Figure 6: **Jump-out events for systems S3 (A) and S4 (B).** System S3 has a slight decrease in contact area during the expansion, but detaches from a relatively large contact area (more than $800\,\mu m^2$) - the middle figure in **A** shows the last FECO recorded before the jump-out event. This behaviour indicates the system is well described by the JKR-model. In system S4, by comparison, we observed a rapid decrease in contact area before jumping out (less than $300\,\mu m^2$), indicating the lipid molecules are constantly peeled off the mica surface before the complete detachment (indicated by the arrows in the middle figure of **B**). This is due to the soft inner DPhyTL layer, giving the lipids more flexibility in the vertical direction.

increases roughly at the pressure level of 10-20 MPa were S3 separates completely, indicating a different detachment path and hence work.

Fourth, for S4 **Figure 5B** further shows representative pressure versus distance profiles during separation for two sets of 5 consecutive repetitions (filled and open round symbols). The two sets differ in their time of exposure to water after the DPhyTL monolayer preparation. Specifically, in a first set of experiments we LB-deposited the outer DPPC layer directly after drying the ethanol-washed DPhyTL monolayer following its deposition. In a second set of experiments the DPhyTL was allowed to rehydrate for >10 hours in water, prior to DPPC deposition in the LB-trough. While the adhesive pressure during separation reaches similar values of about 80-100 MPa, the shape of the pressure versus distance profiles show distinctly different characteristics for the two preparation methods. Specifically, for the

23

system with no additional hydration time the extension δ decreased significantly from 1.5 nm to 0.6 nm upon consecutive probing. Yet it remained constant and about 0.5 nm to 1 nm above the full contour length of the PEG4 for the >10 hours hydrated system.

The decreasing δ for systems with short hydration-time during preparation indicates that DPhyTL in the bilayer architecture may dehydrate under continuous probing, if it is not preconditioned properly by extended hydration of the DPhyTL monolayer. This is consistent with an average hard wall decrease compared to the hydrated system that is within a few Å, yet close to the noise level. For the hydrated system the observation of a plateau of constant force extending further than L_C is interesting and may be explained as follows. We do not observe any decrease in adhesive force or any change of the hard wall thickness, with repeated probing. Thus, we cannot apply an explanation of lipid pluck-out that was observed in other systems with highly adhesive bonds,[9] where a decrease of the interaction force was observed upon consecutive force probing.

We find the thickness of the "stretched bilayer" as it jumps out of contact is by about 1.5–2.0 nm greater than that of its measured thickness under no applied load of about 5.8 nm (using neutron reflectivity[32]). Therefore it may indicate a rehydration of the headgroups and re-establishment of natural undulations during separation in combination with the hydrated PEG4 linker stretching with can explain about 1 nm of the total stretching. This explanation is also consistent with the observed decrease of the plateau length for the non-hydrated DPhyTL system (**Figure 5B** filled circles). That system shows an extension δ that decreases to 5–8 Å after consecutive probing. The value is consistent with a rehydration of the head groups, this time in combination with the PEG extension that may become shorter and shorter upon consecutive probing due to PEG4 dehydration or re-ordering, as the initial hydration state was different from the preconditioned, hydrated S4 (**Figure 5B** open circles). The final PEG4 behavior in the non-hydrated (not preconditioned) state is hence more equivalent to a polymer in a bad solvent. Therefore, in any case the explanation for the extension, δ must be a combination of the polymer stretch and the hydration of both the

lipid headgroups and the PEG4 itself. Compared to tether ligand/receptor separation[9] this different detachment mechanism may also explain the more pronounced L-shape of the separation, as compared to the gradual U-shape observed for ligand/receptor systems.

In conclusion it is interesting to compare the measured data to previous data and simulation work on bilayers contacting solid surfaces. First, the observed adhesion is close to the adhesion observed during hemifusion of lipids by Benz *et al.*[11] and of hydrophobic surfactant monolayers by Helm *et al.*[2] but remains below the equivalent load ($200\,\mathrm{mN/m}$) that would be required to separate two fused bilayers.[39] As such, the hydrophobic attraction maintains the stability of the S3/S4 bilayer systems during separation, and the measured adhesion energy (JKR for S3) and adhesive pressure (for S4) is a good approximation for a DPPC-mica interaction, in rigid and soft support architectures, respectively.

Compared to the work of Anderson, where a DPPC bilayer was approaching a silica surface,[13] our data indicates a jump into an adhesive contact followed by a hydration/undulation repulsion during close approach and high adhesion during separation, for both the S3 and S4 system. This difference evolves from surface roughness, which is different between a silica surface and mica, changing the force profile and adhesion when an SLB is approached.[6,40] In the force profile, roughness asperities can cause the repulsion during the approach of the surfaces to decrease, followed by an earlier increase in the repulsion force than expected as the surfaces begin to make contact at a greater distance and, dependent on the substrate material, the asperities are compressed. Therefore, a well defined attractive jump into contact is absent in a rough system such as silica used by Anderson.[13] Finally, the force profile and work of adhesion of the rigid system is very similar to profiles simulated by Pertsin and Grunze for a PC lipid.[41] While the simulation data also shows a clear effect of undulation and protrusion interactions at small bilayer/mica separations below 1 nm leading to a jump into contact, we find that the jump into contact appears at a larger distance, which may relate to larger VDW forces (induced by the gold support) not present in simulations. Still in close contact we do see a compression over a distance of $D = 0.5$ nm, which appears

to be consistent with undulations and possibly protrusions, while a dehydration contribution cannot be excluded at this point. Here only simulation of this particular system and spectroscopy probe experiments may allow a more detailed molecular level insight.

Conclusions

In this work we explored different ways to reach good stability of SLBs in SFA experiments under highly adhesive conditions. In order to increase the stability under adhesive loads, we tested systems with different inner layers. Using a cationic lipid, DPTAP, to compensate some of the mica charge provided a layer free from holes in the AM-AFM measurements. This is a significant improvement over uncharged lipids, which led to some enhancement of stability. However it was not sufficient under the high loads against mica to maintain a consistent thickness over multiple measurements. Still this is an optional stabilization for experiments at lower adhesive force/pressure, which may be evaluated individually for such experiments. The SAM based SLBs have both shown a good stability under high adhesion (F/R = 60-80 mN/m, or F/A = 80-100 MPa), which is represented by consistent thicknesses and force profiles over multiple measurements. The systems we have introduced compare reasonably well to simulations of related systems.[14] The C_{16} supported DPPC (S3) in particular had a very low roughness (RMS = 0.18 nm), and consistent thickness and adhesion values. However, the surface charge was quite high due to attraction of anions to the interface.

DPhyTL SAM supported DPPC has a low intrinsic surface charge and exhibits undulations on the order of 0.6-1.5 nm if surfaces are prepared without sufficient rehydration time. Hence, for the DPhyTL system a sufficient hydration time is required to fully hydrate the PEG4 chains used in the anchoring system. The fully hydrated DPhyTL supported layer is a very close representation of a floating DPPC bilayer, with undulations and a characteristic bending modulus of $k_b = 2.5 \times 10^{-19}$ J in the range expected for a DPPC bilayer. At the

same time it maintains the greater interaction, to both the support and the outer leaflet, the support layer requires so that the outer DPPC layer remains stable under the high adhesion generated at the DPPC-mica interface. Both SAM supported systems behave as constant charge surfaces. Both systems appear to charge negatively by anion adsorption while the C_{16} supported DPPC (S3) has a higher intrinsic surface charge due to higher van der Waals attraction of anions to the interface.

In summary, SFA measurements provide unique distance dependent interaction profiles enabling molecular scale insight into the forming and breaking of adhesive bonds of four different bilayer model systems. Specifically the DPhyTL-based system offers diverse possibilities for new applications in SFA, including the operando combination of SFA during bond forming and breaking in biomimetic systems with bio- and electrochemical sensing, where DPhyTL membranes are state of the art, providing excellent electrochemical membrane characteristics (see also impedance in the SI, **Figure S5**).

Author contributions

M.V., L.L.E.M., M.L and P.B. planned, discussed, interpreted and conducted research and wrote the manuscript jointly. J.A. assisted with the preparation of DPhyTL membranes, discussed and interpreted results, and co-prepared the manuscript. U.R. joined the project at a late stage, performed the impedance measurements for the DPhyTL based bilayer systems and discussed the research and manuscript.

Acknowledgement

to us. This paper is dedicated to Jacob N. Israelachvili, who pioneered SFA and inspired membrane studies with the SFA.

Supporting Information Available

Surface pressure isotherms for DPPC and DPTAP, FECO to demonstrate the effects of the supporting glue, AFM topographies for the substrates and plots of the adhesion force and impedance spectroscopy for the DPhyTL supported DPPC. This material is available free of charge via the Internet at `http://pubs.acs.org/`.

References

(1) Helm, C. A.; Knoll, W.; Israelachvili, J. N. Measurement of ligand-receptor interactions. *Proceedings of the National Academy of Sciences* **1991**, *88*, 8169–8173.

(2) Helm, C. A.; Israelachvili, J. N.; McGuiggan, P. M. Molecular Mechanisms and Forces Involved in the Adhesion and Fusion of Amphiphilic Bilayers. *Science* **1989**, *246*, 919–922.

(3) Marra, J.; Israelachvili, J. Direct Measurements of Forces between Phosphatidylcholine and Phosphatidylethanolamine Bilayers in Aqueous Electrolyte Solutions. *Biochemistry* **1985**, *24*, 4608–4618.

(4) Israelachvili, J. N.; Wennerström, H. Entropic forces between amphiphilic surfaces in liquids. *The Journal of Physical Chemistry* **1992**, *96*, 520–531.

(5) Helm, C. A.; Israelachvili, J. N. Forces between Phospholipid Bilayers and Relationship to Membrane Fusion. *Methods in Enzymology* **1993**, *220*, 130–143.

(6) Orozco-Alcaraz, R.; Kuhl, T. L. Interaction Forces between DPPC Bilayers on Glass. *Langmuir* **2013**, *29*, 337–343.

(7) Lee, D. W.; Kristiansen, K.; S. H. Donaldson, J.; Cadirov, N.; Banquy, X.; Israelachvili, J. N. Real-time intermembrane force measurements and imaging of lipid domain morphology during hemifusion. *Nat. Commun.* **2015**, *6*.

(8) Kuhl, T. L.; Leckband, D. E.; Lasic, D. D.; Israelachvili, J. N. Modulation of interaction forces between bilayers exposing short-chained ethylene oxide headgroups. *Biophysical Journal* **1994**, *66*, 1479–1488.

(9) Kuhl, T.; Guo, Y.; Alderfer, J. L.; Berman, A. D.; Leckband, D.; Israelachvili, J.; Hui, S. W. Direct Measurement of Polyethylene Glycol Induced Depletion Attraction between Lipid Bilayers. *Langmuir* **1996**, *12*, 3003–3014.

(10) Valtiner, M.; Donaldson, S. H.; Gebbie, M. A.; Israelachvili, J. N. Hydrophobic Forces, Electrostatic Steering, and Acid–Base Bridging between Atomically Smooth Self-Assembled Monolayers and End-Functionalized PEGolated Lipid Bilayers. *Journal of the American Chemical Society* **2011**, *134*, 1746–1753.

(11) Benz, M.; Gutsmann, T.; Chen, N.; Tadmor, R.; Israelachvili, J. N. Correlation of AFM and SFA Measurements Concerning the Stability of Supported Lipid Bilayers. *Biophys. J.* **2004**, *86*.

(12) Andersson, J.; Köper, I. Tethered and Polymer Supported Bilayer Lipid Membranes: Structure and Function. *Membranes* **2016**, *6*.

(13) Anderson, T. H.; Min, Y.; Weirich, K. L.; Zeng, H.; Fygenson, D.; Israelachvili, J. N. Formation of supported bilayers on silica substrates. *Langmuir* **2009**, *25*, 6997–7005.

(14) Pertsin, A.; Grunze, M. Possible mechanism of adhesion in a mica supported phospholipid bilayer. *Journal of Chemical Physics* **2014**, *140*.

(15) Atanasov, V.; Knorr, N.; Duran, R. S.; Ingebrandt, S.; Offenhausser, A.; Knoll, W.; Koeper, I. Membrane on a Chip: A Functional Tethered Lipid Bilayer Membrane on Silicon Oxide Surfaces. *Biophysical journal* **2005**, *3*, 1780–1788.

(16) Vockenroth, I. K.; Atanasova, P. P.; Jenkins, T. A.; Koeper, I. Incorporation of α-

Hemolysin in Different Tethered Bilayer Lipid Membrane Architectures. *Langmuir* **2008**, *2*, 496–502.

(17) Anderson, J.; Knobloch, J.; Pertkins, M.; Holt, S.; Koeper, I. Synthesis and Characterization of Novel Anchorlipids for Tethered Bilayer Lipid Membranes. *Langmuir* **2017**, *18*, 4444–4451.

(18) Goreham, R.; Thompson, V.; Samura, Y.; Gibson, C.; Shapter, J.; Koeper, I. Interaction of Silver Nanoparticles with Tethered Bilayer Lipid Membranes. *Langmuir* **2015**, *21*, 5868–5874.

(19) Anderson, J.; Fuller, M.; Holt, S.; Koeper, I. A tethered bilayer lipid membrane that mimics microbial membranes. *Phys Chem Chem Phys* **2018**, *18*, 12958–12969.

(20) Junghans, A.; Köper, I. Structural Analysis of Tethered Bilayer Lipid Membranes. *Langmuir* **2010**, *26 (13)*.

(21) Schwenzfeier, K.; Erbe, A.; Bilotto, P.; Lengauer, M.; Merola, C.; Cheng, H.; Mears, L.; Valtiner, M. Optimizing multiple beam interferometry in the surface forces apparatus: Novel optics, reflection mode modeling, metal layer thicknesses, birefringence, and rotation of anisotropic layers. *Review of Scientific Instruments* **2019**, *90*.

(22) Israelachvili, J.; Min, Y.; Akbulut, M.; Alig, A.; Carver, G.; Greene, W.; Kristiansen, K.; Meyer, E.; Pesika, N.; Rosenberg, K.; Zeng, H. Recent advances in the surface forces apparatus (SFA) technique. *Reports on Progress in Physics* **2010**, *73*.

(23) Rand, R.; Parsegian, V. Hydration forces between phospholipid bilayers. *Biochimica et Biophysica Acta (BBA) - Reviews on Biomembranes* **1989**, *988*, 351 – 376.

(24) Wong, J. Y.; Kuhl, T. L.; Israelachvili, J. N.; Mullah, N.; Zalipsky, S. Direct Measurement of a Tethered Ligand-Receptor Interaction Potential. *Science* **1997**, *275*, 820–822.

(25) Khan, M. S.; Dosoky, N. S.; Williams, J. D. Engineering Lipid Bilayer Membranes for Protein Studies. *Int. J. Mol. Sci.* **2013**, *14*.

(26) Hui, S.; Viswanathan, R.; Zasadzinski, J.; Israelachvili, J. The structure and stability of phospholipid bilayers by atomic force microscopy. *Biophysical Journal* **1995**, *68*, 171 – 178.

(27) Armstrong, C. L.; Barrett, M. A.; Toppozini, L.; Kučerka, N.; Yamani, Z.; Katsaras, J.; Fragneto, G.; Rheinstädter, M. C. Co-existence of gel and fluid lipid domains in single-component phospholipid membranes. *Soft Matter* **2012**, *8*, 4687–4694.

(28) Fréchette, J.; Kyle Vanderlick, T. Double layer forces over large potential ranges as measured in an electrochemical surface forces apparatus. *Langmuir* **2001**, *17*, 7620–7627.

(29) Valtiner, M.; Banquy, X.; Kristiansen, K.; Greene, G. W.; Israelachvili, J. N. The Electrochemical Surface Forces Apparatus: The Effect of Surface Roughness, Electro-static Surface Potentials, and Anodic Oxide Growth on Interaction Forces, and Friction between Dissimilar Surfaces in Aqueous Solutions. *Langmuir* **2012**, *28*, 13080–13093, PMID: 22877582.

(30) Meuse, C.; Krueger, S.; Majkrzak, C.; Dura, J.; Fu, J.; Connor, J.; Plant, A. Hybrid bilayer membranes in air and water:infrared spectroscopy and neutron reflectivity studies. *Biophysics Journal* **1998**, *74 (3)*.

(31) Tarek, M.; Tu, K.; Klein, M.; Tobias, D. Molecular Dynamics Simulations of Supported Phospholipid/Alkanethiol Bilayer on a Gold (111) Surface. *Biophysics Journal* **1999**, *77 (2)*.

(32) Braunagel, J.; Junghans, A.; Koeper, I. Membrane-based Sensing Approaches. *Australian Journal of Chemistry* **2011**, *64 (1)*.

(33) Popa, I.; Sinha, P.; Finessi, M.; Maroni, P.; Papastavrou, G.; Borkovec, M. Importance of Charge Regulation in Attractive Double-Layer Forces between Dissimilar Surfaces. *Physical Review Letters* **2010**, *140*.

(34) Carnie, S.; Chan, D. Interaction free energy between plates with charge regulation: A linearized model. *Colloid Interface Sci.* **1993**, *161*.

(35) Valtiner, M.; Kristiansen, K.; Greene, G. W.; Israelachvili, J. N. Effect of Surface Roughness and Electrostatic Surface Potentials on Forces Between Dissimilar Surfaces in Aqueous Solution. *Advanced Materials* **2011**, *23*, 2294–2299.

(36) Helfrich, W. Elastic Properties of Lipid Bilayers: Theory and Possible Experiments. *Zeitscrift für Naturforschung C* **1973**, *28*, 693 – 703.

(37) Nagao, M.; Kelley, E.; Ashkar, R.; Bradbury, R.; Butler, P. Probing Elastic and Viscous Properties of Phospholipid Bilayers Using Neutron Spin Echo Spectroscopy. *Journal of Physical Chemistry Letters* **2017**, *8*, 4679 – 4684.

(38) Israelachvili, J. N. *Intermolecular and Surface Forces*, 3rd ed.; Academic Press, 2011.

(39) Helm, C. A.; Israelachvili, J. N.; Mcguiggans, P. M. Role of Hydrophobic Forces in Bilayer Adhesion and Fusion. *Biochemistry* **1992**, *31*, 1794–1805.

(40) Donaldson, S. H.; Valtiner, M.; Gebbie, M. A.; Harada, J.; Israelachvili, J. N. Interactions and visualization of bio-mimetic membrane detachment at smooth and nano-rough gold electrode surfaces. *Soft Matter* **2013**, *9*, 5231.

(41) Pertsin, A.; Grunze, M. Computer simulations of water-mediated force between phospholipid membranes. *Current Opinion in Colloid and Interface Science* **2011**, *16*, 534–541.

SUPPORTING INFORMATION

Interaction profiles and stability of rigid and polymer-tethered lipid bilayer models at highly charged and highly adhesive contacts.

Pierluigi Bilotto, Maximilian Lengauer, Jakob Andersson, Ulrich Ramach, Laura L.E. Mears, Markus Valtiner

Langmuir Blodgett

Figure S1 shows our results from measurements with the LB trough. The surface pressure-area isotherms received for DPPC and DPTAP (**Figure S1A**) were different in shape. For DPPC, one can clearly distinguish between the gas phase, the liquid phase and the condensed phase in the isotherms, since they are separated by plateaus of constant surface pressure, Π, representing the regions where phase transitions takes place. For DPTAP this distinction is not so clear due to the long-range electrostatic repulsion of the charged headgroups, resulting in a more monotonous increase of Π with decreasing area. However, despite the electrostatic headgroup repulsion, a smaller area per molecule was obtained for DPTAP. This is due to the smaller headgroup volume of DPTAP compared to DPPC, resulting in a lower steric repulsion on the short range.

The inset figure of **Figure S1A** shows the area per molecule values received for different mixtures of DPPC and DPTAP in the condensed phase. The scale of the x-axis in this graph is given as the charge per lipid in units of the elementary charge, $e = 1.602 \times 10^{-19}\,\mathrm{C}$, which

directly corresponds to the share of DPTAP in the solution.

In **Figure S1B**, a mica support is considered for the different DPPC/DPTAP mixtures. The charge per lipid is related to the system's overall net surface charge, $\sigma_{net} = \sigma_{Lipids} + \sigma_{Mica}$. The σ_{Lipids} was calculated from the measured area per lipid molecule and the charge per lipid value, defined by the DPPC/DPTAP ratio. The mica substrate was assumed to constitute an ideal lattice, giving $\sigma_{Mica} = 0.35\,\mathrm{C\,m^{-2}}$. For the black fitted line, a coefficient of determination of $R^2 = 0.996$ was received. For realizing full charge compensation, the line would need to cross $\sigma_{net} = 0$, as indicated by the extrapolated blue dashed line.
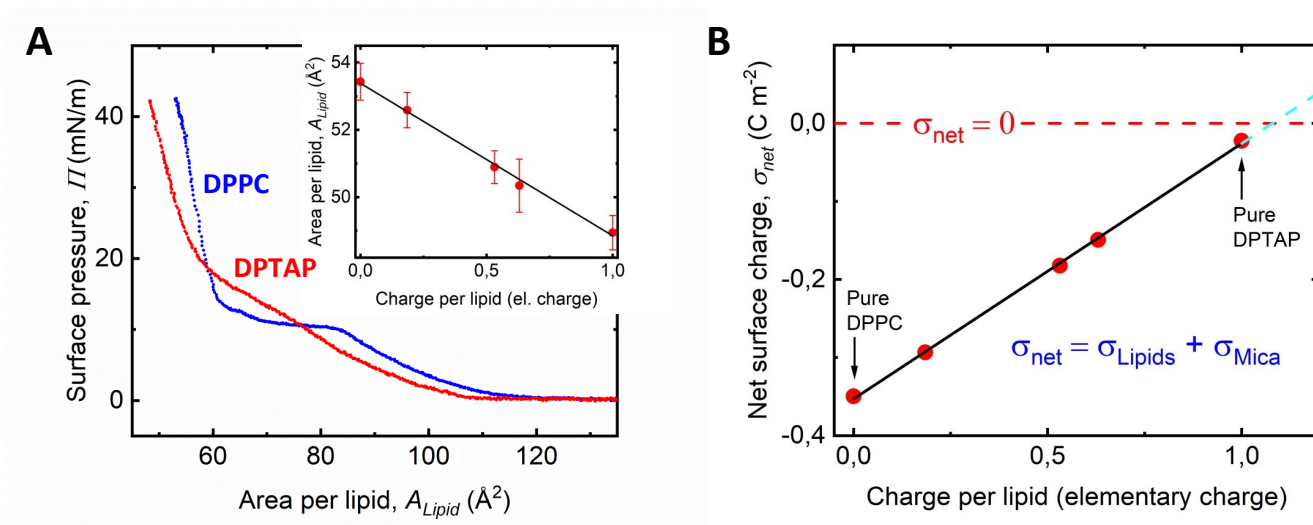
Figure S1: **A** Surface pressure-area isotherms of DPPC (blue) and DPTAP (red) obtained from measurements with the LB trough. Only the compression curves are shown. The inset figure shows the calculated mean area per molecule values for different DPPC/DPTAP mixtures. **B** Net surface charge for a lipid monolayer deposited on a mica substrate, σ_{net}, depending on the charge per lipid for DPPC/DPTAP mixtures. An ideal mica lattice was assumed for the calculation of the given data.
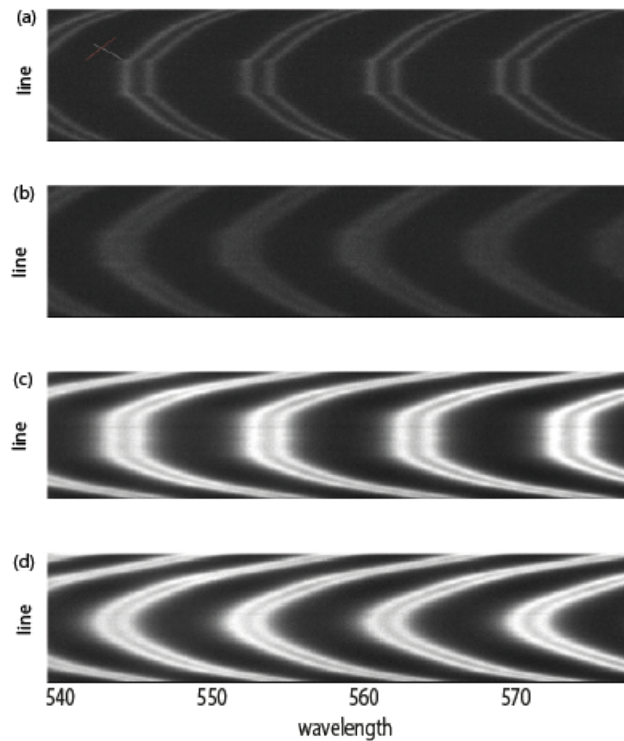
Glue effects

Figure S2: The figure shows the effects of different glues. The pictures(a) and (b) represent FECOs in contact and after the jumping out of the surfaces in an experiment where the UV glue (NOA 81) was used. As we can see from the flattering of the FECO after the jump out event, the deformation of the glue is plastic hence the actual contact area is deformed permanently. The pictures (c) and (d) show the FECOs in contact and after the jumping out of the surfaces during an experiment where the EPO-TEk 377 glue was used. Here the deformation of the glue is elastic because the FECO come back to their original round shaped form.
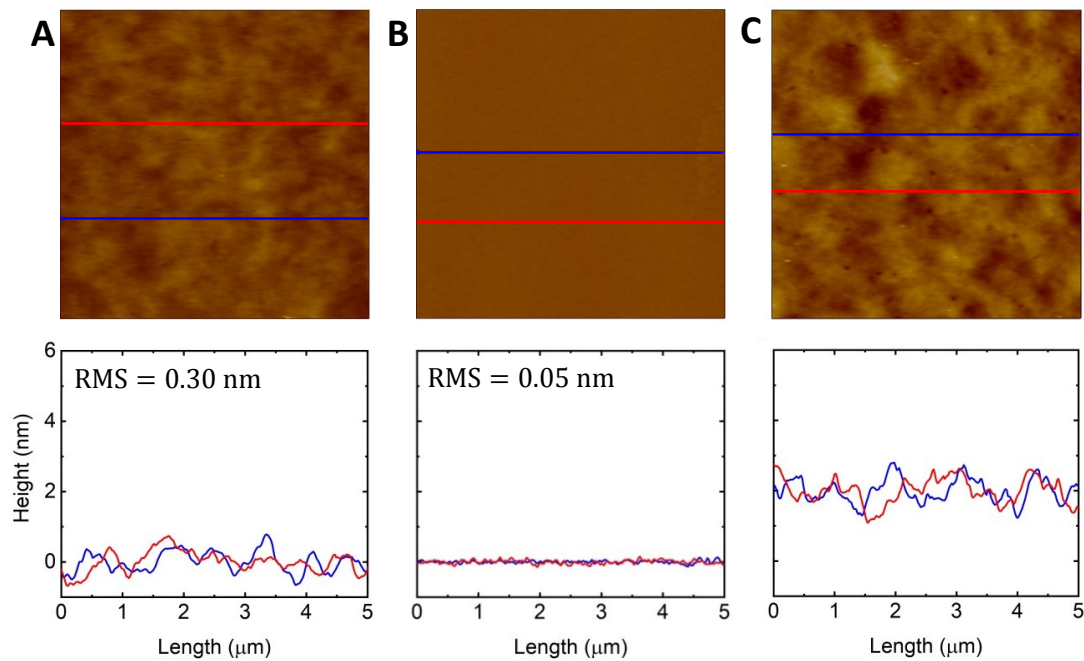
AFM

Figure S3: AFM scan images, performed in 8 mM NaCl solution. Two height profiles at different positions are given for clarity. **A** Gold substrate, fixed with UV-curing adhesive. **B** Gold substrate, fixed with heat curing adhesive. By comparing images **A** and **B** one can see a clear reduction in surface roughness when using the heat curing adhesive.**C** DphyTL on gold attached with heat curing adhesive, recorded in water after less than 1h of immersion time.
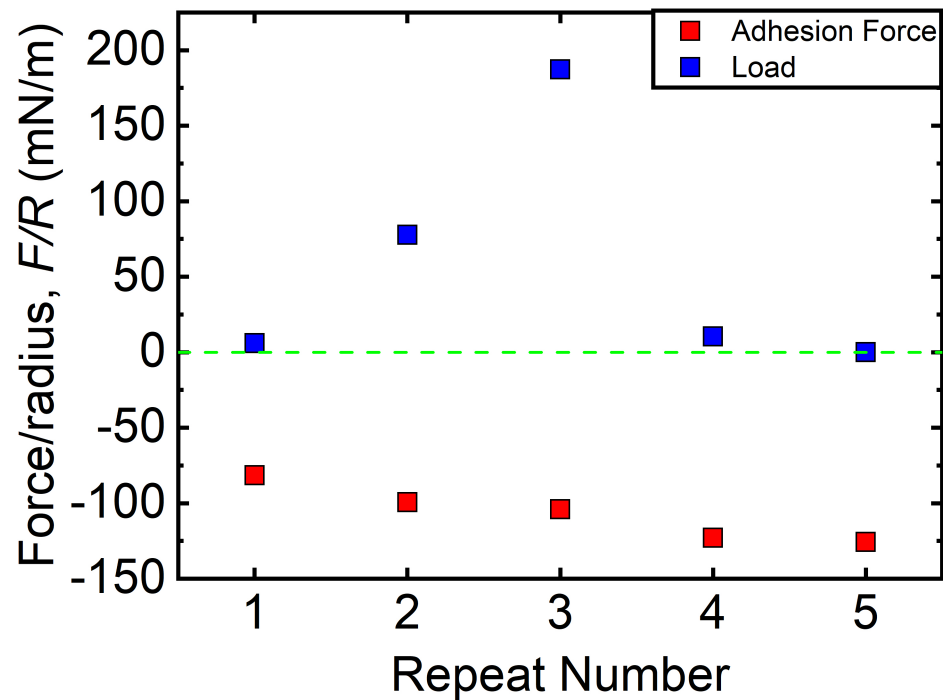
DPhyTL system S4

Figure S4: **Adhesion force and load force applied for each S4 force run (not hydrated).** In the figure, displayed in blue, is the maximum load force applied during approach in each force run and in red the measured adhesion force. There is no direct correlation between the load and the adhesion force.
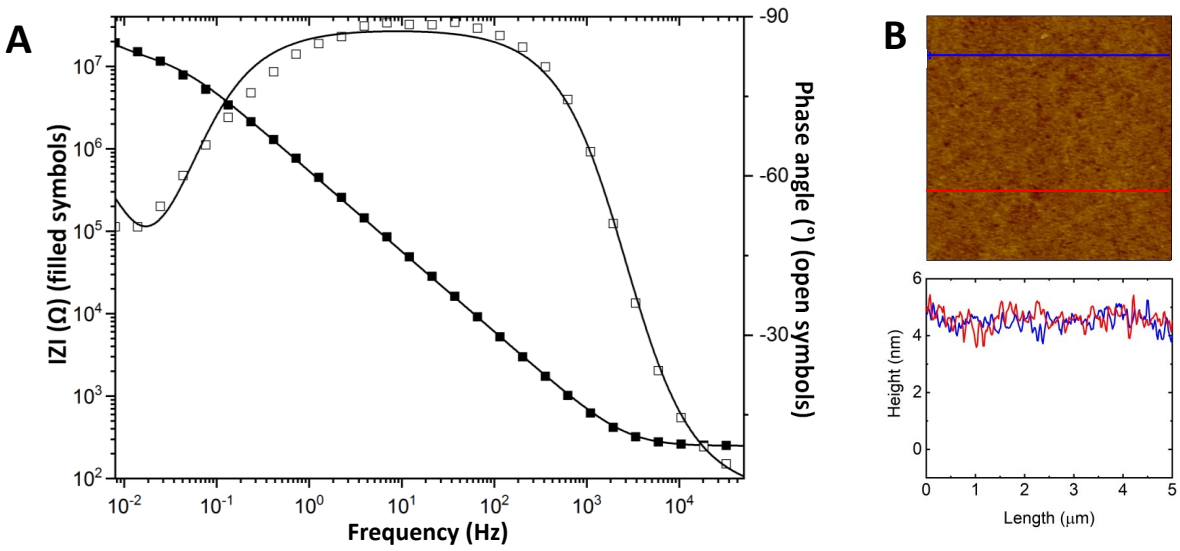
Figure S5: **Impedance, |Z|, measurement on system S4 prepared by vesicle fusion. A** Impedance measurements indicate a stable and entire formation of a bilayer on the substrate. **B** AFM scan image in 8 mM NaCl of system S4, generated by DPPC vesicle fusion compare well with surfaces prepared by LB-deposition. One can see that long-range undulations as they were observed in the DPPC/DPhyTL system prepared by Langmuir deposition shortly after SAM preparation (Figure 3D) are absent in this bilayer. This is due to the longer preparation time, giving the polymers the opportunity to rearrange and hydrate evenly across the layer. Local defects are visible but less predominant compared to Figure 3D (left).